

# Deepfake Detection with Multi-Artifact Subspace Fine-Tuning and Selective Layer Masking

Xiang Zhang, Wenliang Weng, Daoyong Fu, Ziqiang Li, Zhangjie Fu

**Abstract**—Deepfake detection still faces significant challenges in cross-dataset and real-world complex scenarios. The root cause lies in the high diversity of artifact distributions introduced by different forgery methods, while pretrained models tend to disrupt their original general semantic structures when adapting to new artifacts. Existing approaches usually rely on indiscriminate global parameter updates or introduce additional supervision signals, making it difficult to effectively model diverse forgery artifacts while preserving semantic stability. To address these issues, this paper proposes a deepfake detection method based on Multi-Artifact Subspaces and selective layer masks (MASM), which explicitly decouples semantic representations from artifact representations and constrains the fitting strength of artifact subspaces, thereby improving generalization robustness in cross-dataset scenarios. Specifically, MASM applies singular value decomposition to model weights, partitioning pretrained weights into a stable semantic principal subspace and multiple learnable artifact subspaces. This design enables decoupled modeling of different forgery artifact patterns while preserving the general semantic subspace. On this basis, a selective layer mask strategy is introduced to adaptively regulate the update behavior of corresponding network layers according to the learning state of each artifact subspace, suppressing overfitting to any single forgery characteristic. Furthermore, orthogonality constraints and spectral consistency constraints are imposed to jointly regularize multiple artifact subspaces, guiding them to learn complementary and diverse artifact representations while maintaining a stable overall spectral structure. Extensive cross-dataset and robustness experiments demonstrate that MASM achieves significant advantages under various forgery types, compression conditions, and complex distortion scenarios, validating the effectiveness of the proposed strategy.

**Index Terms**—Deepfake Detection, Cross-Dataset Generalization, Artifact Diversity, Multi-Artifact Subspaces, Selective Layer Masking, Semantic-Artifact Decoupling, Spectral Regularization

## I. INTRODUCTION

**I**N recent years, with the rapid advancement of generative artificial intelligence technologies [1]–[4], deepfake techniques have been able to manipulate facial regions with extremely high realism. The resulting forged images and videos can spread rapidly on social media platforms, posing serious threats to personal privacy and exerting profound impacts on the public opinion environment and social trust systems [5]–[10]. In the face of continuously emerging forgery techniques,

This work was supported in part by the National Natural Science Foundation of China under Grant 62202234; in part by the China Postdoctoral Science Foundation under Grant 2023M741778..

Xiang Zhang, Wenliang Weng, Daoyong Fu, Ziqiang Li, and Zhangjie Fu are with the Engineering Research Center of Digital Forensics, Ministry of Education, Nanjing University of Information Science and Technology, Nanjing, Jiangsu 210044, China (e-mail: zhangxiang@nuist.edu.cn; 202412200722@nuist.edu.cn; fudymo@hotmail.com; iceli@mail.ustc.edu.cn; fzj@nuist.edu.cn).

how to construct deepfake detection models that remain robust and highly generalizable under unknown forgery scenarios has become one of the core challenges in the field of digital media forensics.

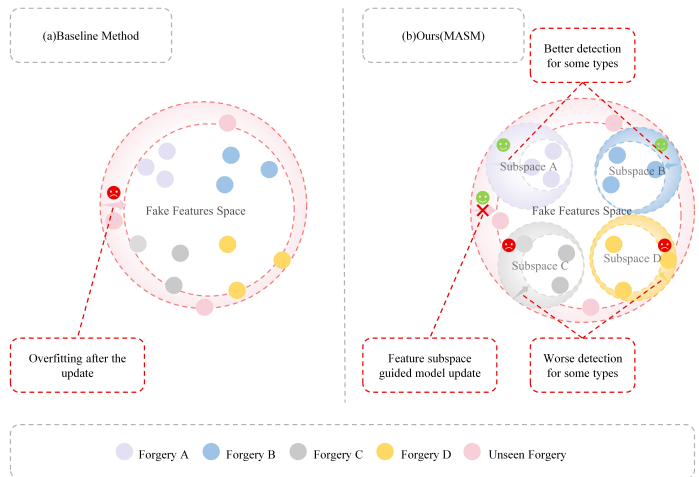


Fig. 1. A simple illustrative example is provided to intuitively demonstrate the proposed deepfake detection method based on multi-artifact subspace fine-tuning and selective layer masking. The baseline method learns within a single feature space, which limits the diversity of forgery patterns it can capture and makes it prone to overfitting to specific forgery types during training, thereby weakening its generalization to unseen forgeries. In contrast, the proposed method partitions the forgery feature space into multiple artifact subspaces to model more diverse forgery types and adaptively controls weight updates according to the learning state of each subspace, effectively alleviating overfitting.

Benefiting from the strong representation capability of convolutional neural networks (CNNs) [11], [12], deep learning-based forgery detection methods have achieved remarkable performance under in-distribution training and testing conditions. However, these methods often rely on local artifact patterns specific to particular forgery algorithms or datasets, and their detection performance degrades significantly when the test distribution shifts. To alleviate such overfitting issues, existing studies mainly enhance model generalization from two perspectives: data synthesis and representation learning.

At the data synthesis level, related methods construct or expand forged samples to cover a broader forgery space, such as boundary blending simulation or latent space augmentation, thereby guiding models to learn discriminative cues shared across different forgery methods [13]–[17]. At the representation learning level, researchers improve robustness to distribution shifts through approaches including spatial-frequency fusion [18], [19], disentangled learning [20], [21], attention mechanisms [22], reconstruction learning [23], and transfer

learning [24]–[27].

However, as illustrated in Fig. 1(a), most existing deepfake detection methods still perform unified modeling of forged samples from different sources and generation mechanisms within a single feature space, while continuously updating the entire network or most layers during training. Such unified modeling and global updating strategies suffer from two intrinsic limitations. First, forgery samples produced by different generation mechanisms often exhibit highly heterogeneous artifact distributions. Compressing them into a single feature space requires this space to simultaneously preserve stable, general semantic structures while accommodating multiple fine-grained artifact patterns. Under these competing optimization objectives, models tend to converge around a small subset of “easy-to-learn” forgeries, leading to feature collapse toward local patterns and weakening the representation capability for other forgery types, especially unknown ones. Second, during the transfer from generic visual representations to the forgery detection task, different network layers exhibit inconsistent learning states. Some layers remain underfitted and benefit from continued updates to extract task-relevant discriminative features, whereas others are already near saturation. Forcing updates on such saturated layers not only yields limited gains but may also introduce overfitting and damage the pretrained semantic structures with good transferability [28]–[33].

To address these issues, we propose MASM, a deepfake detection method based on multi-artifact subspace fine-tuning and selective layer masking, whose core idea is illustrated in Fig. 1(b). Specifically, MASM explicitly constructs multiple artifact subspaces on top of shared pretrained representations through multi-artifact subspace fine-tuning, with each subspace modeling forgery artifact patterns associated with different generation mechanisms and distribution characteristics. Each subspace focuses on capturing a relatively independent class of artifact features, thereby avoiding mutual interference among heterogeneous forgery patterns within a single feature space, while the joint combination of multiple subspaces forms a more expressive and comprehensive artifact representation. Building on this, a selective layer masking mechanism is further introduced to finely control parameter updates during fine-tuning. Since multiple artifact subspaces are derived from subspace decomposition of the same linear mapping and different network layers exhibit significantly different learning states during transfer, when overfitting tendencies are detected in certain subspaces or their corresponding layers, update masks are applied to restrict further optimization of related layers. In this way, feature collapse is suppressed at both the subspace and network layer levels. This strategy effectively expands artifact modeling capacity while preserving the stability of pretrained semantic structures, thereby enhancing generalization under unknown forgery scenarios. The main contributions of this work are summarized as follows:

1. We propose a multi-artifact subspace fine-tuning framework that explicitly decouples forgery artifacts associated with different generation mechanisms into multiple subspaces for modeling, effectively alleviating representation conflicts caused by heterogeneous forgery features within a single representation space and enhancing the ability to model diverse

and unknown forgery patterns.

2. We design a selective layer masking strategy that adaptively controls parameter updates during fine-tuning according to the learning states of network layers, preventing excessive optimization of saturated layers and improving cross-dataset generalization while maintaining the stability of pretrained semantic representations.

3. Extensive experiments under multiple forgery types and cross-dataset transfer settings demonstrate that the proposed MASM method significantly outperforms existing approaches on several mainstream deepfake detection benchmarks, fully validating its robustness and practical value in complex open-world scenarios.

## II. RELATED WORK

### A. Deepfake Generation Methods

Deepfake generation methods primarily manipulate facial identity, expression, or motion to produce forged content in real face images or videos. According to different generation mechanisms, existing approaches can be broadly categorized into face replacement [34]–[36] and face reenactment [37], [38]. Face replacement methods typically achieve identity transfer and swapping through autoencoder-based or graphics-based techniques [34]–[36]. In contrast, face reenactment methods preserve the target identity while driving facial expressions or motions from a source video onto the target face [37], [38]. Although these deepfake methods differ in generation objectives, they generally involve joint modeling of appearance, geometric alignment, and temporal motion. As a result, the generated outputs often introduce multiple types of forgery artifacts [14], [39], [40]. These artifacts exhibit significant variations in spatial distribution and representational levels, giving rise to the characteristic multi-artifact nature of face forgeries.

### B. Data Synthesis-Based Deepfake Detection

In deepfake detection research, data synthesis-based training strategies are widely regarded as effective approaches. Such methods construct or mix synthetic samples to guide models toward learning discriminative cues shared by deepfakes, such as discontinuities along face blending boundaries and statistical inconsistencies between inner and outer facial regions, thereby improving generalization to unseen forgery methods. Early work, FWA [13], adopts a self-blending strategy by applying image transformations such as downsampling to facial regions followed by inverse geometric mapping, in order to simulate warping artifacts introduced during deepfake generation and encourage the model to focus on abnormal patterns caused by geometric distortions. Subsequently, Face X-Ray [14] explicitly constructs blending boundaries to guide detectors to directly learn edge inconsistencies between real and forged regions. SBI [?] performs face swapping using images of the same identity, significantly improving the realism of synthetic data while preserving identity consistency, thus reducing the distribution gap between simple synthetic samples and real forgeries. Building on this, SLADD [15]

combines self-supervised learning with adversarial augmentation to dynamically generate more challenging forged samples, continuously exposing the model to diverse and evolving forgery patterns during training and enhancing its adaptability to complex forgery scenarios. More recently, StA [17] extends the perspective of data synthesis from the image level to the video level by simulating temporally varying facial feature drift through video-level data blending and introducing spatiotemporal adapters to explicitly model such dynamics. Beyond RGB appearance-based synthesis strategies, LSDA [16] further explores the latent space by modeling variations of forgery features within latent representations and their relationships, effectively expanding the distribution of forged samples and providing richer training signals for deepfake detection.

### C. Representation Learning-Based Deepfake Detection

Beyond data synthesis-based strategies, representation learning-based deepfake detection methods constitute another major research direction. These approaches do not rely on explicitly constructing forged samples; instead, they learn discriminative representations that capture intrinsic inconsistencies of deepfakes through feature space modeling, thereby improving generalization across forgery algorithms, compression settings, and demographic variations. Toward this goal, existing studies explore multiple perspectives, including spatial-frequency fusion, feature disentanglement, attention mechanisms, reconstruction consistency, and transfer learning. In spatial-frequency fusion, SFDG [19] jointly models spatial texture cues and frequency-domain statistical features, enhancing sensitivity to high-frequency artifacts and compression distortions. F2Trans [18] further integrates frequency-domain modeling with fine-grained Transformer architectures to capture subtle differences among high-frequency artifacts, thereby improving discriminative capability. To mitigate excessive reliance on specific forgery patterns, disentangled learning methods attempt to separate generic representations from forgery-related representations at the feature level. UCF [20] achieves feature disentanglement via unsupervised contrastive constraints, enabling the model to learn common representations shared across different forgery algorithms. From a fairness generalization perspective, FG [21] introduces feature disentanglement and loss flattening strategies to alleviate performance bias across demographic groups and domains. In artifact modeling, LAA-Net [22] employs localized artifact attention to guide the model toward key forged regions and combines it with a multi-task learning framework, endowing the detector with stronger adaptability across varying compression and quality conditions. In contrast to discriminative learning, RAM [23] adopts a reconstruction-based paradigm that detects forgeries by reconstructing real appearances and measuring reconstruction consistency, thereby identifying forged samples from the perspective of generative consistency. In recent years, with the rise of large-scale pretrained models, transfer learning has become an important means of enhancing cross-domain generalization. FA [24] introduces lightweight adapter modules on top of a frozen CLIP visual encoder to enhance

discrimination of forged regions while preserving semantic consistency. UDD [25] weakens positional and content biases by randomly shuffling and mixing Transformer tokens, encouraging the model to learn more robust, forgery-invariant representations. In addition, MoE-FFD [26] and Effort [27] leverage feature decomposition and subspace modeling to effectively mitigate overfitting while jointly preserving semantic information and learning forgery patterns.

## III. METHODOLOGY

The overall framework of the proposed MASM is illustrated in Fig. 2. The framework is built around two core ideas: \*multi-artifact subspace modeling\* and \*selective layer masking\*. Within a unified training pipeline, multi-artifact subspace fine-tuning, selective layer masking, and subspace constraint mechanisms are jointly incorporated. By performing controlled fine-tuning on task-sensitive layers and decoupling representations of different forgery artifacts at the subspace level, MASM effectively enhances the modeling capability for diverse deepfake traces while preserving the stability of pretrained semantic representations.

### A. Multi-Artifact Subspace Fine-Tuning

Previous studies [27], [41]–[43] have shown that the knowledge embedded in pretrained models exhibits distinctive spectral energy distribution properties in the parameter space: high-energy spectral directions typically correspond to stable and well-transferable generic semantic structures, whereas low-energy spectral directions are more sensitive to task- or domain-specific variations. Motivated by this observation, we introduce singular value decomposition (SVD) at the parameter level to explicitly decompose model weight matrices into a semantic subspace and multiple artifact subspaces. Unlike Effort [27], which models a single artifact representation within the residual subspace, we further subdivide it into multiple mutually independent artifact subspaces and explicitly encourage each subspace to focus on different types of forgery traces through orthogonality constraints, thereby enhancing the model’s capacity to capture complex forgery patterns.

Specifically, let the weight matrix of a certain layer in the pretrained visual backbone be denoted as  $W \in \mathbb{R}^{d_{in} \times d_{out}}$ . Applying singular value decomposition (SVD) yields

$$W = U \Sigma V^\top, \quad (1)$$

where  $\Sigma = \text{diag}(\sigma_1, \sigma_2, \dots, \sigma_R)$  is the diagonal matrix of singular values sorted in descending order by energy, and  $U$  and  $V$  are the corresponding left and right singular vector matrices, respectively.

We retain the top  $r$  singular components to construct a low-rank semantic subspace dominated by high-energy spectral directions:

$$W_{\text{Semantic}} = U_{[:,1:r]} \Sigma_{[1:r,1:r]} V_{[:,1:r]}^\top, \quad (2)$$

which preserves the global semantic structure learned by the pretrained model and remains frozen throughout training to prevent disruption of generic representations.

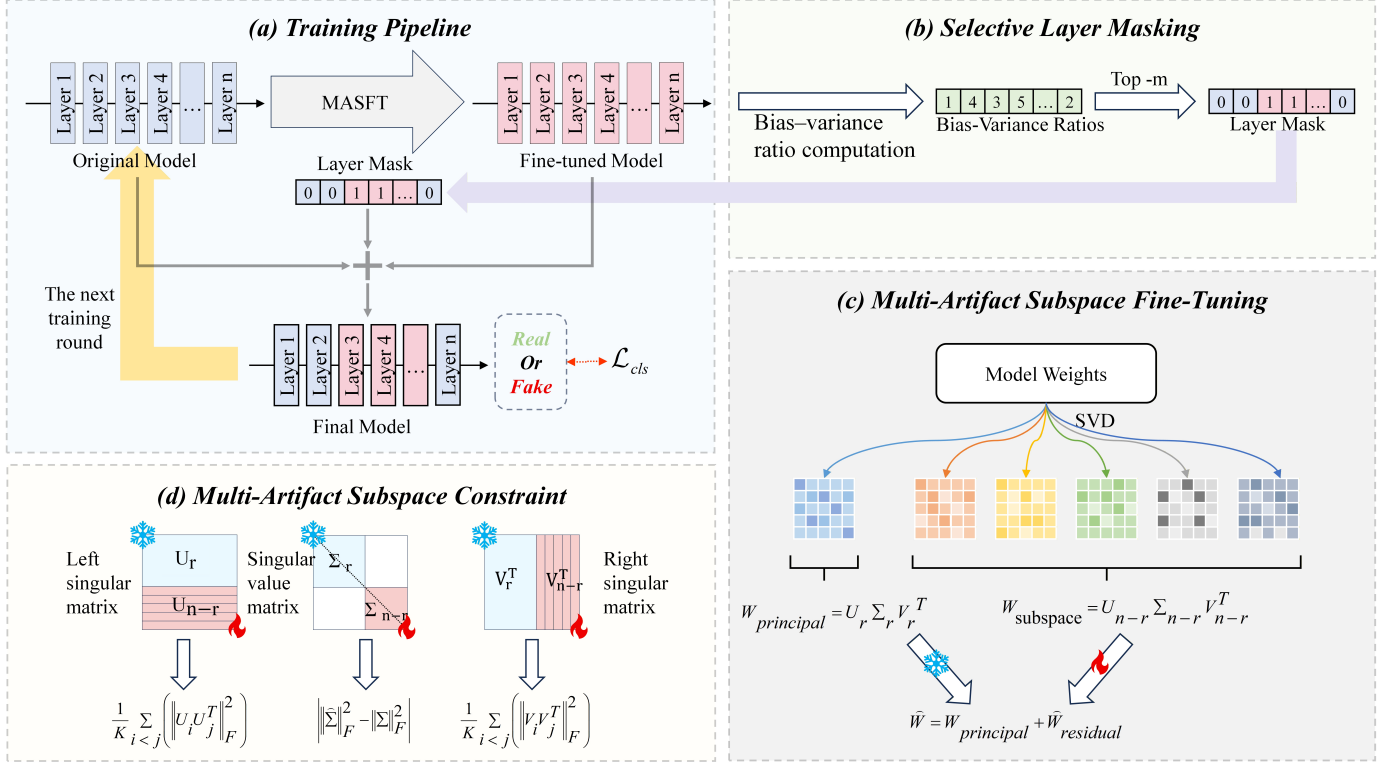


Fig. 2. Overall overview of the proposed MASM framework.(a) **Training pipeline**. Starting from the original model, the model is iteratively optimized by introducing the Multi-Artifact Subspace Fine-Tuning (MASFT) mechanism, together with a selective layer masking strategy that progressively updates key layer parameters, resulting in the final discriminative model.(b) **Selective layer masking**. The bias–variance ratio is computed for each network layer, and the Top-K layers are adaptively selected based on the ranking results to construct a binary layer mask that guides the subsequent fine-tuning process.(c) **Multi-artifact subspace fine-tuning**. Model weights are decomposed into a principal subspace and artifact-related subspaces via singular value decomposition (SVD), enabling targeted fine-tuning within multiple artifact subspaces.(d) **Multi-artifact subspace constraints**. Orthogonality and spectral consistency constraints are imposed on the left singular vectors, singular values, and right singular vectors to enhance the decoupling among different artifact subspaces.

The remaining singular components are further partitioned into  $K$  mutually independent artifact subspaces, each represented as  $W_k = U_k \Sigma_k V_k^\top$ , which together constitute the learnable part of the model:

$$W_{\text{Artifact}} = \sum_{k=1}^K U_k \Sigma_k V_k^\top. \quad (3)$$

Based on this design, the proposed Multi-Artifact Subspace Modeling (MASM) framework updates only  $W_{\text{Artifact}}$ , while the semantic subspace  $W_{\text{Semantic}}$  serves as a stable anchor to constrain the overall representation from drifting in irrelevant directions. The effective weight used for forward propagation can thus be expressed as the additive combination of the semantic and artifact subspaces:

$$\hat{W} = W_{\text{Semantic}} + \hat{W}_{\text{Artifact}}. \quad (4)$$

### B. Selective Layer Masking

Existing studies have shown that fine-tuning only a subset of model layers or adopting layer-wise differentiated learning rates can significantly improve model generalization performance [44]–[46]. Motivated by this observation, under the Multi-Artifact Subspace Modeling (MASM) framework, we design a Selective Layer Mask (SLM) mechanism for each

layer involved in fine-tuning. This mechanism adaptively modulates the update strength of different layers, enabling a fine-grained balance between model stability and adaptability.

Specifically, let  $B$  denote a mini-batch randomly sampled from the training data. The parameter update rule is unified as

$$\theta^{(l,t)} \leftarrow \theta^{(l,t-1)} + M^{(l,t)} \mathbf{d}^{(l,t)}, \quad (5)$$

where  $t$  denotes the iteration index,  $\theta^{(l,t)}$  represents the parameter subset of the  $l$ -th layer at iteration  $t$ ,  $\mathbf{d}^{(l,t)}$  is the update direction, and  $M^{(l,t)} \in \{0, 1\}$  is the selective layer mask indicating whether the  $l$ -th layer is activated for updating at the current iteration. The update direction follows standard gradient descent:

$$\mathbf{d}^{(l,t)} = -\eta \mathbf{g}^{(l,t)}, \quad (6)$$

where  $\eta \in \mathbb{R}$  is the learning rate, and  $\mathbf{g}^{(l,t)} = \nabla_{\theta^{(l,t)}} \mathcal{L}(\theta^{(l,t)})$  denotes the mini-batch gradient computed on  $B$  with respect to the predefined loss function  $\mathcal{L}$ .

Within this update framework, the selective layer mask  $M^{(l,t)}$  is explicitly embedded into the parameter update process to impose structured control over layer-wise updates. When  $M^{(l,t)} = 1$ , the  $l$ -th layer is activated and participates in parameter updating at iteration  $t$ ; when  $M^{(l,t)} = 0$ , the layer remains frozen in the current iteration, thereby avoiding unnecessary perturbations to its parameters.

The key challenge lies in adaptively generating appropriate masks for different layers. To this end, inspired by bias-variance analysis [47], we characterize the stability of layer-wise update signals using mini-batch gradient statistics. Specifically, we define the bias  $b$  and variance  $v$  of the mini-batch gradients, and use their ratio as a measure of layer-wise update reliability:

$$b = \left\| \mathbb{E}[\mathbf{g}^{(l,t)}] \right\|^2, \quad v = \text{tr}(\mathbb{V}[\mathbf{g}^{(l,t)}]). \quad (7)$$

To reduce computational overhead and improve statistical stability, exponential moving averages are employed to estimate the first- and second-order moments of the gradients:

$$\mu_i^{(l,t)} = \alpha \mu_i^{(l,t-1)} + (1 - \alpha) g_i^{(l,t)}, \quad (8)$$

$$\sigma_i^{(l,t)} = \alpha \sigma_i^{(l,t-1)} + (1 - \alpha) (g_i^{(l,t)})^2, \quad (9)$$

where  $\mu_i^{(l,t)}$  and  $\sigma_i^{(l,t)}$  denote the estimates of the first- and second-order moments of the gradient, respectively,  $\alpha \in [0, 1]$  is the exponential smoothing coefficient, and  $g_i^{(l,t)}$  denotes the  $i$ -th component of the gradient vector  $\mathbf{g}^{(l,t)}$ .

Based on these statistics, the bias-variance ratio of the  $l$ -th layer at iteration  $t$  is defined as

$$\text{BVG}^{(l,t)} = \frac{\sum_i (\mu_i^{(l,t)})^2}{\sum_i (\sigma_i^{(l,t)} - (\mu_i^{(l,t)})^2)}. \quad (10)$$

Finally, the layer mask is generated according to the  $\text{BVG}^{(l,t)}$  values across layers. In the current implementation, the top- $m$  layers with the largest  $\text{BVG}^{(l,t)}$  values are selected to participate in updating:

$$M^{(l,t)} = \begin{cases} 1, & \text{if } l \in \text{Top-}m(\text{BVG}^{(l,t)}), \\ 0, & \text{otherwise.} \end{cases} \quad (11)$$

### C. Objective Function

**Subspace Orthogonality Constraint.** To prevent different artifact subspaces from learning redundant representations, we explicitly impose orthogonality constraints among artifact subspaces to encourage them to capture complementary and diverse forgery traces. Let the weight component of the  $k$ -th artifact subspace be represented via singular value decomposition as  $(U_k, \Sigma_k, V_k)$ , where  $U_k \in \mathbb{R}^{d_{\text{out}} \times r_k}$  and  $V_k \in \mathbb{R}^{r_k \times d_{\text{in}}}$  denote the left and right singular vector matrices, respectively.

For any two distinct artifact subspaces  $(i, j)$ , orthogonality constraints are simultaneously imposed in both the left and right singular vector spaces. The orthogonality loss is defined as

$$\mathcal{L}_{\text{orth}} = \frac{2}{K(K-1)} \sum_{i < j} \left( \|V_i V_j^\top\|_F^2 + \|U_i^\top U_j\|_F^2 \right), \quad (12)$$

where  $K$  denotes the number of artifact subspaces and  $\|\cdot\|_F$  is the Frobenius norm.

**Spectral Consistency Constraint.** During multi-artifact subspace fine-tuning, in the absence of explicit constraints, the model may alter the overall spectral energy distribution of the weight matrix by amplifying or suppressing singular

values, thereby damaging the stable semantic structure learned in the pretrained model. To this end, we introduce a spectral consistency constraint to limit the deviation of spectral energy before and after fine-tuning:

$$\mathcal{L}_{\text{spec}} = \left\| \hat{W} \right\|_F^2 - \|W\|_F^2, \quad (13)$$

where  $\hat{W}$  denotes the weight matrix obtained after the current iteration,  $W$  is the corresponding pretrained weight matrix, and  $\|\cdot\|_F$  denotes the Frobenius norm.

**Classification Loss.** To supervise the deepfake detection task, we adopt the standard cross-entropy loss as the classification objective:

$$\mathcal{L}_{\text{cls}} = -\frac{1}{N} \sum_{i=1}^N (y_i \log p_i + (1 - y_i) \log(1 - p_i)), \quad (14)$$

where  $y_i \in \{0, 1\}$  denotes the ground-truth label of the  $i$ -th sample,  $p_i$  represents the predicted probability that the sample belongs to the fake class, and  $N$  is the number of samples in the current mini-batch.

**Overall Loss.** The final optimization objective is defined as

$$\mathcal{L}_{\text{total}} = \mathcal{L}_{\text{cls}} + \lambda_1 \frac{1}{n} \sum_{i=1}^n \mathcal{L}_{\text{orth}}^{(i)} + \lambda_2 \frac{1}{n} \sum_{i=1}^n \mathcal{L}_{\text{spec}}^{(i)}, \quad (15)$$

where  $\lambda_1$  and  $\lambda_2$  are hyperparameters that balance structural regularization and task optimization, and  $n$  denotes the number of layers where multi-subspace fine-tuning is applied.

## IV. EXPERIMENTS

### A. Experimental Setup

**Datasets:** To comprehensively evaluate the generalization capability of the proposed method under diverse scenarios, we conduct experiments on multiple widely used deepfake detection benchmarks, including FaceForensics++ (FF++) [39], CelebDF (CDF) [36], DFDC Preview (DFDC-P) [48], the Deepfake Detection Challenge dataset (DFDC) [49], and DeepfakeDetection (DFD) [50]. Among them, FF++ is a large-scale dataset containing over 1.8 million manipulated frames generated from 1,000 original videos. The forged samples are produced using four representative facial manipulation methods, namely DeepFakes [35], Face2Face [37], FaceSwap [34], and NeuralTexture [38], all based on the same set of source videos. FF++ provides three compression levels: raw (uncompressed), lightly compressed (c23), and heavily compressed (c40). Following common practice in prior work, we use FF++ (c23) for training, while the remaining four datasets are exclusively used for cross-dataset evaluation.

**Implementation Details:** All experiments are conducted on a single NVIDIA RTX 4090 GPU and implemented using PyTorch 2.1.2. The visual backbone is initialized with the pretrained CLIP ViT-L/14 model [51]. Within the proposed MASM framework, linear layers of the backbone are adapted using the Multi-Artifact Subspace Fine-Tuning (MASFT) strategy, while all other parameters remain frozen during training to preserve the global semantic representations learned during pretraining. To further evaluate the adaptability of MASM across different visual representations, we additionally

compare its performance using multiple pretrained visual backbones, with the results summarized in Table ???. All experiments follow the default evaluation protocol provided by DeepfakeBench [52]. During training, the Adam optimizer is employed with an initial learning rate of  $2 \times 10^{-4}$ , a batch size of 32, and a total of 10 training epochs. For each video sample, 32 frames are uniformly sampled during both training and testing. The overall training objective consists of the standard cross-entropy loss together with two subspace regularization terms, namely the orthogonality constraint and the spectral consistency constraint, which are weighted by  $\lambda_1 = 1.0$  and  $\lambda_2 = 1.0$ , respectively.

**Evaluation Metrics:** To comprehensively assess detection performance, we report the Area Under the Curve (AUC) at both the frame level and the video level, enabling systematic comparisons between the proposed method and representative existing approaches. In addition, we also report Average Precision (AP) and Equal Error Rate (EER) to provide a more comprehensive and objective evaluation of model performance.

### B. Generalization Evaluation

For generalization evaluation, we follow a widely adopted protocol: models are trained on FF++ (c23) [39] and tested on other datasets, such as CDF [36] and DFDC [49]. In the reported results, frame-level AUC is provided for frame-based forgery detection methods, while video-level AUC is reported for video-based detection methods, ensuring fair comparisons across different types of approaches.

**Frame-level AUC Evaluation:** Table I shows the frame-level AUC comparison results for models trained on FF++ (c23) and evaluated on multiple cross-dataset benchmarks. It can be observed that the proposed MASM exhibits strong cross-domain generalization performance across all test datasets. On the DFDC [49] and DFD [50] datasets, MASM achieves frame-level AUC scores of 0.84412 and 0.94778, respectively, both surpassing existing state-of-the-art methods. On the CDF [36] and DFDCP [48] datasets, MASM attains AUC scores of 0.89463 and 0.88380, respectively, which are only slightly lower than those achieved by FA [24], with an average performance gap of merely 0.00548.

It is worth noting that FA [24] introduces an additional mask prediction branch to guide the model to focus on facial boundary regions, thereby providing certain advantages for face-swapping-based forgeries. However, this method relies on extra pixel-level annotations, imposing higher requirements on the training data and limiting its practical applicability. In contrast, the proposed MASM does not require any explicit mask supervision and can be trained using only raw images, while achieving strong performance across diverse forgery datasets, which clearly demonstrates its superior generalization capability.

**Video-level AUC Evaluation:** Table II presents the comparison results of video-level generalization performance across datasets under the same training setting. It can be observed that the proposed MASM achieves the best performance on all test datasets, with an average video-level AUC of 0.92985, significantly outperforming existing state-of-the-art methods.

Specifically, on the DFDC [49] and DFD [50] datasets, MASM improves upon the second-best method, Effort [27], by more than 2%, and outperforms StA [17] by approximately 1.6%, indicating stronger cross-domain generalization capability in complex video forgery scenarios.

It is worth noting that StA [17] is a representative video-level detection method that explicitly models inter-frame inconsistencies to capture temporal forgery cues, thereby achieving strong performance under multi-frame inputs. In contrast, the proposed MASM does not rely on dense temporal modeling or additional video-level modules; instead, it effectively captures forgery traces using only single-frame images, while still consistently surpassing StA in overall performance. This further validates the robustness and effectiveness of MASM for cross-domain deepfake detection.

### C. Robustness Evaluation

To evaluate the robustness of the proposed method under real-world conditions, we adopt the same perturbation settings as in [60] and introduce six representative types of distortions into the test videos, including color saturation variation, color contrast variation, block-wise distortion, Gaussian blur, JPEG compression, and Gaussian noise. For each distortion type, five different intensity levels are applied to systematically simulate quality degradations that may occur in practical scenarios. Fig. 3 presents a comparison of video-level AUC results between the proposed method and FA [24], ProDet [54], and Effort [27]. The results show that MASM consistently maintains stable detection performance across all distortion types and intensity levels, exhibiting substantially better overall robustness than the competing methods. In contrast, the other approaches suffer from noticeable performance degradation under certain high-intensity distortions, whereas MASM demonstrates stronger resistance to various perturbations, further confirming its applicability and robustness in complex real-world environments.

### D. Ablation Study and Analysis

**Method ablation:** To evaluate the contribution of each core component to the overall performance, we conduct ablation studies on the proposed Multi-Artifact Subspace Fine-Tuning (MASFT) and the Selective Layer Mask (SLM). Specifically, while keeping the remaining network architecture and training configuration strictly identical, we remove one component at a time to ensure a fair comparison. Model performance is evaluated using three metrics: Area Under the Curve (AUC), Average Precision (AP), and Equal Error Rate (EER). The results are summarized in Table III.

It is worth noting that our method only modifies the linear projections within the self-attention modules. Therefore, in the ablation setting without MASFT, we fully fine-tune the self-attention linear layers of the CLIP model, while keeping all other network parameters frozen, to maintain comparability across different experimental settings. The ablation results show that MASFT contributes most significantly to performance improvement, indicating that multi-artifact subspace

TABLE I

COMPARISON WITH EXISTING METHODS. WE REPORT THE **FRAME-LEVEL AUC** OF MODELS TRAINED ON FF++ (C23) AND EVALUATED ON DIFFERENT DATASETS. METHODS MARKED WITH \* DENOTE REPRODUCED RESULTS BASED ON THEIR PUBLICLY AVAILABLE MODELS AND WEIGHTS. IN THE TABLE, **BOLD** AND UNDERLINED ENTRIES INDICATE THE BEST AND SECOND-BEST PERFORMANCE, RESPECTIVELY. THE REMAINING RESULTS ARE REPORTED IN THE ORIGINAL PAPERS OR IN DEEPCODEBENCH [52].

Method	Venue	CDF	DFDCP	DFDC	DFD	Average
UCF [20]	ICCV 2023	0.77900	0.75900	0.71900	0.80700	0.76600
IID [53]	CVPR 2023	0.76900	0.76200	0.69500	0.79300	0.75475
ProDet* [54]	NeurIPS 2024	0.84193	0.77435	0.69732	0.84784	0.79036
LSDA [16]	CVPR 2024	0.83000	0.81500	0.73600	0.88000	0.81525
IDCNet [55]	TIFS 2024	0.80890	0.74090	0.72440	0.84710	0.78033
FreqDebias [56]	CVPR 2025	0.83600	0.82400	0.74100	0.86800	0.81725
Effort* [27]	ICML 2025	0.87853	0.83563	0.82261	0.92239	0.86479
UDD [25]	AAAI 2025	0.86900	0.85600	0.75800	0.91000	0.84825
FA [24]	CVPR 2025	<b>0.89948</b>	<b>0.88991</b>	<u>0.84260</u>	<u>0.93289</u>	<u>0.89122</u>
<b>MASM</b>	–	<u>0.89463</u>	<u>0.88380</u>	<b>0.84412</b>	<b>0.94778</b>	<b>0.89258</b>

TABLE II

COMPARISON WITH EXISTING METHODS. WE REPORT THE **VIDEO-LEVEL AUC** OF MODELS TRAINED ON FF++ (C23) AND EVALUATED ON DIFFERENT DATASETS. METHODS MARKED WITH \* DENOTE REPRODUCED RESULTS BASED ON THEIR PUBLICLY AVAILABLE MODELS AND WEIGHTS. IN THE TABLE, **BOLD** AND UNDERLINED ENTRIES INDICATE THE BEST AND SECOND-BEST PERFORMANCE, RESPECTIVELY. THE REMAINING RESULTS ARE REPORTED IN THE ORIGINAL PAPERS OR IN DEEPCODEBENCH [52].

Method	Venue	CDF	DFDCP	DFDC	DFD	Average
UCF [20]	ICCV 2023	0.83700	0.77000	0.74200	0.86700	0.80400
TALL* [57]	ICCV 2023	0.63951	0.56148	0.52201	0.50843	0.55786
IID* [53]	CVPR 2023	0.78723	0.71688	0.70866	0.82761	0.76009
AltFreezing* [58]	CVPR 2023	0.80146	0.66689	0.64015	0.71838	0.70672
ProDet* [54]	NeurIPS 2024	0.92616	0.82823	0.72517	0.90139	0.84524
CDFA [59]	ECCV 2024	0.93800	0.83000	0.83000	0.95400	0.88800
LSDA [16]	CVPR 2024	0.87500	0.81200	0.70100	0.88100	0.81725
Effort* [27]	ICML 2025	0.92703	0.85692	<u>0.85061</u>	0.95721	0.89794
UDD [25]	AAAI 2025	0.93100	0.88100	0.81200	0.95500	0.89475
StA [17]	CVPR 2025	<u>0.94700</u>	<u>0.90900</u>	0.84300	<u>0.96500</u>	<u>0.91600</u>
<b>MASM</b>	–	<b>0.95230</b>	<b>0.91386</b>	<b>0.87133</b>	<b>0.98191</b>	<b>0.92985</b>

modeling effectively enhances the model’s feature representation capacity. When MASFT and SLM are jointly enabled, the model achieves the best performance across all evaluation metrics, validating the complementarity of the two mechanisms within a unified training framework.

In addition, for the two settings without multi-artifact subspace fine-tuning, since the number of training epochs is fixed to 10, the models have not fully converged under the current training configuration, and their performance continues to improve toward the end of training. This observation partly explains why the performance of using only SLM is slightly lower than that of the setting without either component. Such degradation mainly stems from insufficient convergence caused by the limited number of trainable parameters, rather

than from an inherent limitation of the SLM itself.

**Loss ablation:** To evaluate the contribution of each loss term to the overall model performance, we conduct step-by-step ablation experiments on the orthogonality constraint  $\mathcal{L}_{\text{orth}}$  and the spectral consistency constraint  $\mathcal{L}_{\text{spec}}$ . Specifically, while keeping the network architecture and training configuration strictly identical, we remove one loss term at a time to ensure a fair comparison. Model performance is evaluated using AUC, AP, and EER, and the complete results are summarized in Table IV.

From the experimental results, it can be observed that when both  $\mathcal{L}_{\text{orth}}$  and  $\mathcal{L}_{\text{spec}}$  are jointly applied, the model achieves the best performance across all evaluation metrics. Compared with the setting that does not use either loss term, the average AUC

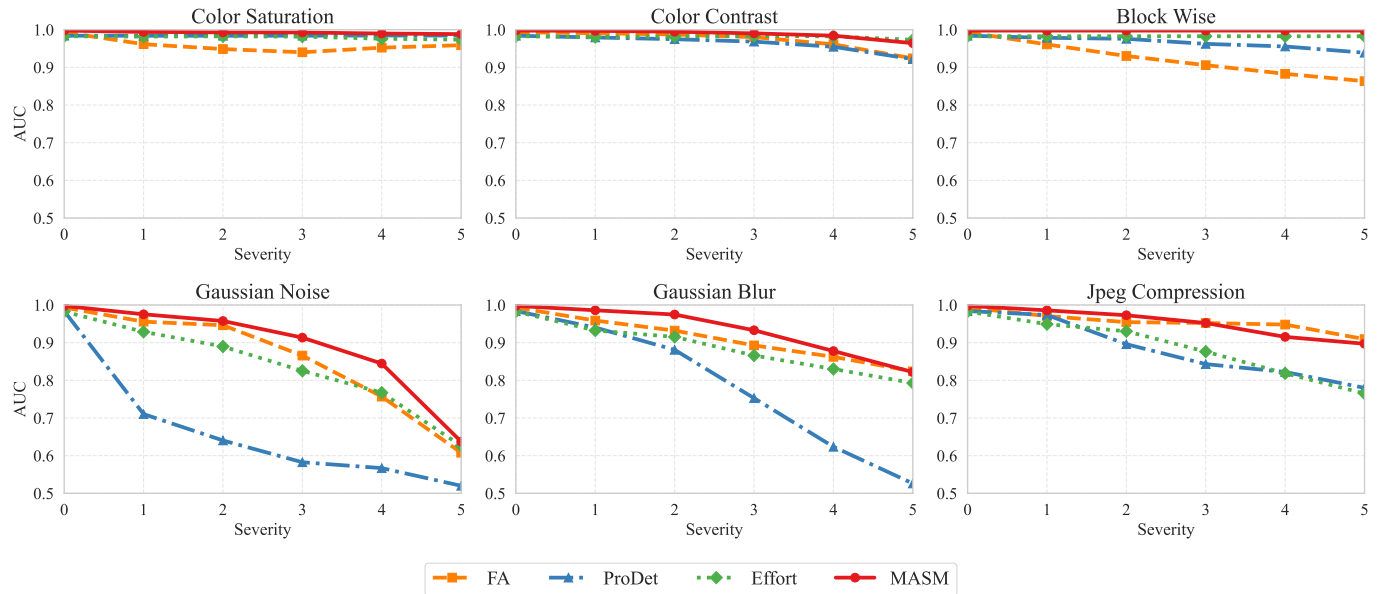


Fig. 3. Robustness evaluation results. We compare our method with FA [24], ProDet [54], and Effort [27] in terms of video-level AUC under six types of distortions and five different intensity levels. It can be observed that MASM maintains stable and consistently high detection performance across different distortion types and severity levels.

TABLE III

ABLATION EXPERIMENTS ON THE EFFECTIVENESS OF **MASFT** AND **SLM**. ALL MODELS ARE TRAINED ON THE FF++ (C23) DATASET [39] AND EVALUATED UNDER CROSS-DATASET SETTINGS. THE EVALUATION METRICS ARE REPORTED AS AUC | AP | EER (FRAME-LEVEL). THE TABLE ALSO PRESENTS THE AVERAGE PERFORMANCE ACROSS ALL DATASETS (AVERAGE), AND THE BEST RESULTS ARE HIGHLIGHTED IN **BOLD**.

MASFT	SLM	CDF			DFDCP			DFDC			DFD			Average		
		AUC	AP	EER												
✗	✗	0.623	0.729	67.6	0.647	0.700	40.3	0.576	0.595	44.7	0.533	0.905	47.6	0.595	0.732	50.0
✓	✗	0.892	<b>0.944</b>	<b>18.6</b>	0.864	0.927	22.8	0.829	0.861	25.2	0.939	0.992	12.7	0.881	0.931	19.8
✗	✓	0.617	0.742	43.0	0.573	0.579	47.0	0.516	0.525	49.8	0.511	0.894	49.0	0.554	0.685	47.2
✓	✓	<b>0.895</b>	0.943	18.9	<b>0.884</b>	<b>0.939</b>	<b>20.1</b>	<b>0.844</b>	<b>0.873</b>	<b>24.1</b>	<b>0.948</b>	<b>0.994</b>	<b>11.6</b>	<b>0.893</b>	<b>0.937</b>	<b>18.7</b>

improves by approximately 2%, AP increases by about 1.2%, and EER is reduced by around 1.8%. These results indicate that the two subspace constraints exhibit strong complementarity during joint optimization, effectively enhancing both the model’s discriminative capability and training stability.

**Effect of the number of artifact subspaces  $K$ :** This experiment aims to analyze the impact of the number of artifact subspaces  $K$  on model performance, thereby exploring the trade-off between subspace partition granularity and model capacity. Under the same training settings, we vary  $K$  over  $\{1, 3, 5, 7, 9\}$  and conduct frame-level AUC evaluation across four cross-dataset scenarios. The experimental results are summarized in Table V.

From the results, it can be observed that as  $K$  increases, the model performance improves notably in the early stages. However, when  $K > 5$ , the overall performance tends to saturate or even slightly decline. When  $K = 5$ , the model achieves frame-level AUC scores of 0.895, 0.884, 0.844, and 0.948 on the CDF, DFDCP, DFDC, and DFD datasets, respectively, with an average performance of **0.893**, which is the best among all configurations.

These observations indicate that a moderate partitioning

of artifact subspaces helps enhance the model’s ability to capture diverse forgery artifacts, whereas an excessive number of subspaces may introduce redundant features and increase optimization difficulty, thereby negatively affecting overall generalization performance. Based on this analysis, we adopt  $K = 5$  as the default setting in subsequent experiments to achieve a balanced trade-off between performance and computational efficiency.

**Effect of the Number of Fine-Tuned Layers  $m$  in the Selective Layer Mask:** This experiment aims to analyze the impact of the number of fine-tuned layers  $m$  in the selective layer mask (SLM) strategy on model performance, thereby exploring the relationship between the depth of parameter updates and feature generalization capability. Under the same training settings, we set  $m$  to  $\{1, 4, 16, 48, 96\}$  and conduct frame-level AUC evaluations across four cross-dataset scenarios, with the results summarized in Table VI.

The backbone network used in this study is CLIP ViT-L/14 [51], which consists of 24 Vision Transformer blocks. Each block contains a self-attention module, and each self-attention module includes four linear layers, resulting in a total of 96 linear layers that can be fine-tuned. When  $m = 96$ , this

TABLE IV

ABLATION EXPERIMENTS ON THE EFFECTIVENESS OF THE  $\mathcal{L}_{\text{orth}}$  AND  $\mathcal{L}_{\text{spec}}$  CONSTRAINTS. ALL MODELS ARE TRAINED ON THE FF++ (c23) DATASET [39] AND EVALUATED IN CROSS-DATASET SETTINGS. FRAME-LEVEL EVALUATION METRICS ARE REPORTED AS AUC, AP, AND EER. THE TABLE ALSO REPORTS THE AVERAGE PERFORMANCE ACROSS ALL DATASETS (AVERAGE), AND THE BEST RESULTS ARE SHOWN IN BOLD.

$\mathcal{L}_{\text{orth}}$	$\mathcal{L}_{\text{spec}}$	CDF			DFDCP			DFDC			DFD			Average		
		AUC	AP	EER												
×	×	0.865	0.925	22.0	0.859	0.925	22.9	0.831	0.862	25.3	0.937	0.992	13.2	0.873	0.926	20.8
✓	×	0.869	0.929	21.7	0.868	0.928	21.7	0.823	0.856	25.5	0.945	0.993	12.4	0.876	0.927	20.3
×	✓	0.875	0.932	20.7	0.874	0.931	20.6	0.823	0.855	26.0	0.946	0.993	12.0	0.880	0.928	19.8
✓	✓	<b>0.895</b>	<b>0.943</b>	<b>18.9</b>	<b>0.884</b>	<b>0.939</b>	<b>20.1</b>	<b>0.844</b>	<b>0.873</b>	<b>24.1</b>	<b>0.948</b>	<b>0.993</b>	<b>11.6</b>	<b>0.893</b>	<b>0.937</b>	<b>18.7</b>

TABLE V

EFFECT OF THE NUMBER OF ARTIFACT SUBSPACES  $K$  ON THE FRAME-LEVEL AUC AND AVERAGE PERFORMANCE ACROSS DIFFERENT DATASETS.

K	CDF	DFDCP	DFDC	DFD	Average
1	0.873	0.879	0.829	0.943	0.881
3	0.872	0.853	0.841	0.946	0.878
<b>5</b>	<b>0.895</b>	<b>0.884</b>	<b>0.844</b>	<b>0.948</b>	<b>0.893</b>
7	0.888	0.874	0.832	0.946	0.885
9	0.894	0.873	0.829	0.945	0.885

setting is equivalent to fully fine-tuning all self-attention linear layers.

As the number of fine-tuned layers increases, model performance shows a clear improvement in the early stage and reaches its optimum at  $m = 16$ , achieving an average AUC of **0.893**. This indicates that a moderate level of layer-wise fine-tuning can effectively enhance the model's adaptability to cross-domain forgery features while preserving the pretrained semantic structure. However, when  $m > 16$ , the performance shows a slight degradation, suggesting that excessively deep parameter updates may adversely affect the stability of pretrained representations and thus weaken overall generalization performance. Based on these observations, we adopt  $m = 16$  as the default setting in subsequent experiments to achieve a reasonable balance between performance and training stability.

TABLE VI

EFFECT OF THE NUMBER OF FINE-TUNED LAYERS  $m$  IN THE SELECTIVE LAYER MASK ON THE FRAME-LEVEL AUC AND AVERAGE PERFORMANCE ACROSS DIFFERENT DATASETS.

m	CDF	DFDCP	DFDC	DFD	Average
1	0.807	0.752	0.791	0.925	0.819
4	0.893	0.862	<b>0.848</b>	0.944	0.887
<b>16</b>	<b>0.895</b>	<b>0.884</b>	0.844	<b>0.948</b>	<b>0.893</b>
48	0.884	0.875	0.828	0.939	0.881
96	0.892	0.864	0.829	0.939	0.881

**Effect of pretrained vision foundation models:** We investigate the impact of different pretrained vision foundation models (VFs) on the performance of the proposed MASM framework. Specifically, we evaluate four representative models, including BEiT ViT-B/16 [61], BEiT ViT-L/16 [61], CLIP

ViT-B/16 [51], and CLIP ViT-L/14 [51], with CLIP ViT-L/14 serving as the default backbone in our main experiments. The results are summarized in Table VII.

The results show that CLIP-based models consistently outperform the BEiT variants across all test datasets. This performance gap can be mainly attributed to the differences in their pretraining paradigms. BEiT learns visual representations through masked image modeling, which emphasizes local reconstruction and pixel-level consistency. In contrast, CLIP is pretrained using large-scale image-text contrastive learning, enabling the model to acquire more discriminative and semantically consistent high-level representations under cross-modal supervision. As a result, CLIP exhibits stronger semantic transferability in cross-domain deepfake detection tasks.

Moreover, from the perspective of model capacity, ViT-L/14 further improves overall performance compared with ViT-B/16, indicating that higher-capacity visual encoders enable the multi-artifact subspace decomposition module in MASM to capture more stable and discriminative artifact features.

TABLE VII

EFFECT OF VISION FOUNDATION MODELS (VFs) ON THE FRAME-LEVEL AUC AND AVERAGE PERFORMANCE ACROSS DIFFERENT DATASETS.

VFs	CDF	DFDCP	DFDC	DFD	Average
BEiT ViT-B/16	0.667	0.766	0.628	0.692	0.688
BEiT ViT-L/16	0.732	0.781	0.737	0.828	0.769
CLIP ViT-B/16	0.837	0.800	0.792	0.907	0.834
CLIP ViT-L/14	<b>0.895</b>	<b>0.884</b>	<b>0.844</b>	<b>0.948</b>	<b>0.893</b>

## V. CONCLUSION

We propose MASM, a deepfake detection method based on multi-artifact subspace fine-tuning and selective layer masking, aiming to improve generalization across datasets and complex real-world scenarios. To address the limitations of existing approaches, which tend to disrupt general semantic structures during fine-tuning and struggle to model diverse forgery artifacts, MASM builds a controlled and interpretable fine-tuning framework from the perspectives of parameter-space decomposition and layer-wise update control. Specifically, MASM applies singular value decomposition to self-attention linear layers, partitioning pretrained weights into a stable semantic principal subspace and multiple learnable artifact subspaces, thereby enabling decoupled modeling of different

forgery patterns while preserving global semantic stability. In addition, a selective layer masking strategy is introduced to adaptively restrict the scope of parameter updates based on layer importance, mitigating semantic drift caused by over-fine-tuning. Within a unified training framework, orthogonality and spectral consistency constraints are jointly imposed to regularize the artifact subspaces, enhancing their independence and stability. Extensive cross-dataset experiments, robustness evaluations, and systematic ablation studies demonstrate that MASM consistently achieves strong and stable detection performance under diverse forgery types and complex perturbations without relying on additional supervision, significantly outperforming existing methods and validating the effectiveness and practicality of multi-artifact subspace modeling with selective parameter updates for deepfake detection.

## REFERENCES

- [1] T. Karras, S. Laine, and T. Aila, “A style-based generator architecture for generative adversarial networks,” *2019 IEEE/CVF Conference on Computer Vision and Pattern Recognition (CVPR)*, pp. 4396–4405, 2018.
- [2] I. J. Goodfellow, J. Pouget-Abadie, M. Mirza, B. Xu, D. Warde-Farley, S. Ozair, A. C. Courville, and Y. Bengio, “Generative adversarial networks,” *2014 14th International Conference on Computing Communication and Networking Technologies (ICCCNT)*, pp. 1–7, 2021.
- [3] R. Rombach, A. Blattmann, D. Lorenz, P. Esser, and B. Ommer, “High-resolution image synthesis with latent diffusion models,” *2022 IEEE/CVF Conference on Computer Vision and Pattern Recognition (CVPR)*, pp. 10674–10685, 2021.
- [4] J. Ho, A. Jain, and P. Abbeel, “Denoising diffusion probabilistic models,” in *Advances in Neural Information Processing Systems*, vol. 33, 2020, pp. 6840–6851.
- [5] R. M. Chesney and D. K. Citron, “Deep fakes: A looming challenge for privacy, democracy, and national security,” *California Law Review*, vol. 107, p. 1753, 2018.
- [6] H.-P. Lee, Y.-J. Yang, T. S. von Davier, J. Forlizzi, and S. Das, “Deepfakes, phrenology, surveillance, and more! a taxonomy of ai privacy risks,” *Proceedings of the 2024 CHI Conference on Human Factors in Computing Systems*, 2023.
- [7] A. Busacca and M. A. Monaca, “Deepfake: Creation, purpose, risks,” in *Innovations and economic and social changes due to artificial intelligence: the state of the art*. Springer, 2023, pp. 55–68.
- [8] J. Kietzmann, L. W. Lee, I. P. McCarthy, and T. C. Kietzmann, “Deepfakes: Trick or treat?” *Business Horizons*, vol. 63, no. 2, pp. 135–146, 2020.
- [9] C. Vaccari and A. Chadwick, “Deepfakes and disinformation: Exploring the impact of synthetic political video on deception, uncertainty, and trust in news,” *Social Media + Society*, vol. 6, 2020.
- [10] T. Wang, X. Liao, K.-p. Chow, X. Lin, and Y. Wang, “Deepfake detection: A comprehensive survey from the reliability perspective,” *ACM Computing Surveys*, vol. 57, pp. 1–35, 2022.
- [11] F. Chollet, “Xception: Deep learning with depthwise separable convolutions,” *2017 IEEE Conference on Computer Vision and Pattern Recognition (CVPR)*, pp. 1800–1807, 2016.
- [12] M. Tan and Q. V. Le, “Efficientnet: Rethinking model scaling for convolutional neural networks,” *arXiv preprint arXiv:1905.11946*, 2019.
- [13] Y. Li and S. Lyu, “Exposing deepfake videos by detecting face warping artifacts,” in *CVPR Workshops*, 2018.
- [14] L. Li, J. Bao, T. Zhang, H. Yang, D. Chen, F. Wen, and B. Guo, “Face x-ray for more general face forgery detection,” *2020 IEEE/CVF Conference on Computer Vision and Pattern Recognition (CVPR)*, pp. 5000–5009, 2019.
- [15] L. Chen, Y. Zhang, Y. Song, L. Liu, and J. Wang, “Self-supervised learning of adversarial example: Towards good generalizations for deepfake detection,” *2022 IEEE/CVF Conference on Computer Vision and Pattern Recognition (CVPR)*, pp. 18689–18698, 2022.
- [16] Z. Yan, Y. Luo, S. Lyu, Q. Liu, and B. Wu, “Transcending forgery specificity with latent space augmentation for generalizable deepfake detection,” *2024 IEEE/CVF Conference on Computer Vision and Pattern Recognition (CVPR)*, pp. 8984–8994, 2023.
- [17] Z. Yan, Y. Zhao, S. Chen, X. Fu, T. Yao, S. Ding, and L. Yuan, “Generalizing deepfake video detection with plug-and-play: Video-level blending and spatiotemporal adapter tuning,” *2025 IEEE/CVF Conference on Computer Vision and Pattern Recognition (CVPR)*, pp. 12615–12625, 2024.
- [18] C. Miao, Z. Tan, Q. Chu, H. Liu, H. Hu, and N. Yu, “F2trans: High-frequency fine-grained transformer for face forgery detection,” *IEEE Transactions on Information Forensics and Security*, vol. 18, pp. 1039–1051, 2023.
- [19] Y. Wang, K. Yu, C. Chen, X. Hu, and S. Peng, “Dynamic graph learning with content-guided spatial-frequency relation reasoning for deepfake detection,” *2023 IEEE/CVF Conference on Computer Vision and Pattern Recognition (CVPR)*, pp. 7278–7287, 2023.
- [20] Z. Yan, Y. Zhang, Y. Fan, and B. Wu, “Ucf: Uncovering common features for generalizable deepfake detection,” *2023 IEEE/CVF International Conference on Computer Vision (ICCV)*, pp. 22355–22366, 2023.
- [21] L. Lin, X. He, Y. Ju, X. Wang, F. Ding, and S. Hu, “Preserving fairness generalization in deepfake detection,” *2024 IEEE/CVF Conference on Computer Vision and Pattern Recognition (CVPR)*, pp. 16815–16825, 2024.
- [22] D. Nguyen, N. Mejri, I. P. Singh, P. Kuleshova, M. Astrid, A. Kacem, E. Ghorbel, and D. Aouada, “Laa-net: Localized artifact attention network for quality-agnostic and generalizable deepfake detection,” *2024 IEEE/CVF Conference on Computer Vision and Pattern Recognition (CVPR)*, pp. 17395–17405, 2024.
- [23] J. Tian, Y. Cai, X. Wang, P. Chen, Z. Xiao, J. Dai, J. Han, and Y. Chai, “Real appearance modeling for more general deepfake detection,” in *European Conference on Computer Vision*, 2024.
- [24] X. Cui, Y. Li, A. Luo, J. Zhou, and J. Dong, “Forensics adapter: Adapting clip for generalizable face forgery detection,” *2025 IEEE/CVF Conference on Computer Vision and Pattern Recognition (CVPR)*, pp. 19207–19217, 2025.
- [25] X. Fu, Z. Yan, T. Yao, S. Chen, and X. Li, “Exploring unbiased deepfake detection via token-level shuffling and mixing,” in *AAAI Conference on Artificial Intelligence*, 2025.
- [26] C. Kong, A. Luo, S. Xia, Y. Yu, H. Li, and A. C. Kot, “Moe-ffd: Mixture of experts for generalized and parameter-efficient face forgery detection,” *arXiv preprint arXiv:2404.08452*, 2024.
- [27] Z. Yan, J. Wang, Z. Wang, P. Jin, K.-Y. Zhang, S. Chen, T. Yao, S. Ding, B. Wu, and L. Yuan, “Orthogonal subspace decomposition for generalizable ai-generated image detection,” in *International Conference on Machine Learning*, 2024.
- [28] R. Geirhos, J.-H. Jacobsen, C. Michaelis, R. S. Zemel, W. Brendel, M. Bethge, and F. Wichmann, “Shortcut learning in deep neural networks,” *Nature Machine Intelligence*, vol. 2, pp. 665 – 673, 2020.
- [29] J. Yosinski, J. Clune, Y. Bengio, and H. Lipson, “How transferable are features in deep neural networks?” *ArXiv*, vol. abs/1411.1792, 2014.
- [30] Z. Li and D. Hoiem, “Learning without forgetting,” *IEEE Transactions on Pattern Analysis and Machine Intelligence*, vol. 40, pp. 2935–2947, 2016.
- [31] Z. Li, P. Xia, H. Sun, Y. Zeng, W. Zhang, and B. Li, “Explore the effect of data selection on poison efficiency in backdoor attacks,” *IEEE Transactions on Dependable and Secure Computing*, vol. 22, pp. 7430–7447, 2023.
- [32] Z. Li, C. Wang, X. Rui, C. Xue, J. Leng, Z. Fu, and B. Li, “Peer is your pillar: A data-unbalanced conditional gans for few-shot image generation,” *IEEE Transactions on Circuits and Systems for Video Technology*, vol. 35, pp. 1303–1317, 2025.
- [33] Z. Li, H. Sun, P. Xia, B. Xia, X. Rui, W. Zhang, and B. Li, “A proxy attack-free strategy for practically improving the poisoning efficiency in backdoor attacks,” *IEEE Transactions on Information Forensics and Security*, vol. 19, pp. 9730–9743, 2023.
- [34] (2021) Faceswap. Accessed 2020-09-03. [Online]. Available: <https://github.com/MarekKowalski/FaceSwap>
- [35] (2020) Deepfakes. Accessed 2020-09-02. [Online]. Available: <https://www.github.com/deepfakes/faceswap>
- [36] Y. Li, X. Yang, P. Sun, H. Qi, and S. Lyu, “Celeb-df: A large-scale challenging dataset for deepfake forensics,” *2020 IEEE/CVF Conference on Computer Vision and Pattern Recognition (CVPR)*, pp. 3204–3213, 2019.
- [37] J. Thies, M. Zollhöfer, M. Stamminger, C. Theobalt, and M. Nießner, “Face2face: Real-time face capture and reenactment of rgb videos,” *2016 IEEE Conference on Computer Vision and Pattern Recognition (CVPR)*, pp. 2387–2395, 2016.

- [38] J. Thies, M. Zollhöfer, and M. Nießner, “Deferred neural rendering: Image synthesis using neural textures,” *AcM Transactions on Graphics (TOG)*, vol. 38, no. 4, pp. 1–12, 2019.
- [39] A. Rössler, D. Cozzolino, L. Verdoliva, C. Riess, J. Thies, and M. Nießner, “Faceforensics++: Learning to detect manipulated facial images,” *2019 IEEE/CVF International Conference on Computer Vision (ICCV)*, pp. 1–11, 2019.
- [40] L. Chai, D. Bau, S.-N. Lim, and P. Isola, “What makes fake images detectable? understanding properties that generalize,” in *European Conference on Computer Vision*, 2020.
- [41] A. Aghajanyan, L. Zettlemoyer, and S. Gupta, “Intrinsic dimensionality explains the effectiveness of language model fine-tuning,” in *Annual Meeting of the Association for Computational Linguistics*, 2020.
- [42] F. Zhang and M. Pilanci, “Spectral adapter: Fine-tuning in spectral space,” *arXiv preprint arXiv:2405.13952*, 2024.
- [43] M. Thamm, M. Staats, and B. Rosenow, “Random matrix analysis of deep neural network weight matrices,” *Physical Review E*, vol. 106, p. 054124, 2022.
- [44] Z. Shen, Z. Liu, J. Qin, M. Savvides, and K.-T. Cheng, “Partial is better than all: Revisiting fine-tuning strategy for few-shot learning,” *arXiv preprint arXiv:2102.03983*, 2021.
- [45] Y. Lee, A. S. Chen, F. Tajwar, A. Kumar, H. Yao, P. Liang, and C. Finn, “Surgical fine-tuning improves adaptation to distribution shifts,” *arXiv preprint arXiv:2210.11466*, 2022.
- [46] J. Tian, X. Dai, C.-Y. Ma, Z. He, Y.-C. Liu, and Z. Kira, “Trainable projected gradient method for robust fine-tuning,” *2023 IEEE/CVF Conference on Computer Vision and Pattern Recognition (CVPR)*, pp. 7836–7845, 2023.
- [47] M. Tomita, I. Sato, R. Kawakami, N. Inoue, S. Ikehata, and M. Tanaka, “A simple finetuning strategy based on bias-variance ratios of layer-wise gradients,” in *Asian Conference on Computer Vision*, 2024.
- [48] B. Dolhansky, R. Howes, B. Pflaum, N. Baram, and C. Canton-Ferrer, “The deepfake detection challenge (dfdc) preview dataset,” *arXiv preprint arXiv:1910.08854*, 2019.
- [49] B. Dolhansky, J. Bitton, B. Pflaum, J. Lu, R. Howes, M. Wang, and C. Canton-Ferrer, “The deepfake detection challenge (dfdc) dataset,” *arXiv preprint arXiv:2006.07397*, 2020.
- [50] “Contributing data to deepfake detection,” 2019. [Online]. Available: <https://ai.googleblog.com/2019/09/contributing-data-to-deepfakedetection.html>
- [51] A. Radford, J. W. Kim, C. Hallacy, A. Ramesh, G. Goh, S. Agarwal, G. Sastry, A. Askell, P. Mishkin, J. Clark, G. Krueger, and I. Sutskever, “Learning transferable visual models from natural language supervision,” in *International Conference on Machine Learning*, 2021.
- [52] Z. Yan, Y. Zhang, X. Yuan, S. Lyu, and B. Wu, “Deepfakebench: A comprehensive benchmark of deepfake detection,” *arXiv preprint arXiv:2307.01426*, 2023.
- [53] B. Huang, Z. Wang, J. Yang, J. Ai, Q. Zou, Q. Wang, and D. Ye, “Implicit identity driven deepfake face swapping detection,” in *Proceedings of the IEEE/CVF conference on computer vision and pattern recognition*, 2023, pp. 4490–4499.
- [54] J. Cheng, Z. Yan, Y. Zhang, Y. Luo, Z. Wang, and C. Li, “Can we leave deepfake data behind in training deepfake detector?” *Advances in Neural Information Processing Systems*, vol. 37, pp. 21979–21998, 2024.
- [55] Z. Wang, Y. Chen, Y. Yao, M. Han, W. Xing, and M. Li, “Idcnet: Image decomposition and cross-view distillation for generalizable deepfake detection,” *IEEE Transactions on Information Forensics and Security*, 2025.
- [56] H. Kashiani, N. A. Talemi, and F. Afghah, “Freqdebias: Towards generalizable deepfake detection via consistency-driven frequency debiasing,” in *Proceedings of the IEEE/CVF Conference on Computer Vision and Pattern Recognition (CVPR)*, June 2025, pp. 8775–8785.
- [57] Y. Xu, J. Liang, G. Jia, Z. Yang, Y. Zhang, and R. He, “Tall: Thumbnail layout for deepfake video detection,” in *Proceedings of the IEEE/CVF international conference on computer vision*, 2023, pp. 22658–22668.
- [58] Z. Wang, J. Bao, W. Zhou, W. Wang, and H. Li, “Altfreezing for more general video face forgery detection,” in *Proceedings of the IEEE/CVF conference on computer vision and pattern recognition*, 2023, pp. 4129–4138.
- [59] Y. Lin, W. Song, B. Li, Y. Li, J. Ni, H. Chen, and Q. Li, “Fake it till you make it: Curricular dynamic forgery augmentations towards general deepfake detection,” in *European Conference on Computer Vision*, 2024.
- [60] L. Jiang, W. Wu, R. Li, C. Qian, and C. C. Loy, “Deeperforensics-1.0: A large-scale dataset for real-world face forgery detection,” in *2020 IEEE/CVF Conference on Computer Vision and Pattern Recognition (CVPR)*, 2020, pp. 2886–2895.
- [61] H. Bao, L. Dong, and F. Wei, “Beit: Bert pre-training of image transformers,” *arXiv preprint arXiv:2106.08254*, 2021.